

Angewandte Chemie

Eine Zeitschrift der Gesellschaft Deutscher Chemiker

GDCh

www.angewandte.de

Akzeptierter Artikel

Titel: A Hybrid Supramolecular Polymeric Nanomedicine for Cascade-Amplified Synergetic Cancer Therapy

Autoren: Kai Yang, Shaolong Qi, Xinyang Yu, Bing Bai, Xueyan Zhang, Zhengwei Mao, Feihe Huang, and Guocan Yu

Dieser Beitrag wurde nach Begutachtung und Überarbeitung sofort als "akzeptierter Artikel" (Accepted Article; AA) publiziert. Die deutsche Übersetzung wird gemeinsam mit der endgültigen englischen Fassung erscheinen. Die endgültige englische Fassung (Version of Record) wird ehestmöglich nach dem Redigieren und einem Korrekturgang als Early-View-Beitrag erscheinen und kann sich naturgemäß von der AA-Fassung unterscheiden. Leser sollten daher die endgültige Fassung, sobald sie veröffentlicht ist, verwenden. Für die AA-Fassung trägt der Autor die alleinige Verantwortung.

Zitierweise: *Angew. Chem. Int. Ed.* **2022**, e202203786

Link zur VoR: <https://doi.org/10.1002/anie.202203786>

RESEARCH ARTICLE

A Hybrid Supramolecular Polymeric Nanomedicine for Cascade-Amplified Synergetic Cancer Therapy

Kai Yang,⁺ Shaolong Qi,⁺ Xinyang Yu, Bing Bai, Xueyan Zhang, Zhengwei Mao, Feihe Huang, and Guocan Yu*

K. Yang, Dr. S. Qi, Dr. X. Yu, Dr. B. Bai, X. Zhang, Prof. Dr. G. Yu
Key Laboratory of Bioorganic Phosphorus Chemistry & Chemical Biology
Department of Chemistry, Tsinghua University
Beijing 100084, P. R. China
E-mail: guocanyu@mail.tsinghua.edu.cn

Prof. Dr. F. Huang

State Key Laboratory of Chemical Engineering, Stoddart Institute of Molecular Science, Department of Chemistry, Zhejiang University, Hangzhou 310027, P. R. China;

ZJU-Hangzhou Global Scientific and Technological Innovation Center, Hangzhou, 311215, P. R. China;

Green Catalysis Center and College of Chemistry, Zhengzhou University, Zhengzhou 450001, P. R. China

Prof. Dr. Z. Mao

Key Laboratory of Precision Diagnosis and Treatment for Hepatobiliary and Pancreatic Tumor of Zhejiang Province, the Second Affiliated Hospital, School of Medicine, Zhejiang University, MOE Key Laboratory of Macromolecular Synthesis and Functionalization, Department of Polymer Science and Engineering, Zhejiang University, Hangzhou, Zhejiang 310027, P. R. China.

* These authors contributed equally.

Abstract: Supramolecular nanomedicines have shown unparalleled merits in cancer therapy, but their clinical translation is greatly hampered by monotonous therapeutic modality and unsatisfactory antitumor performance. Herein, a hybrid supramolecular polymeric nanomedicine (**SNPs**) is developed based on β -cyclodextrin/camptothecin (CPT) host-guest molecular recognition and iron-carboxylate coordination. Iron ions stabilizing **SNPs** catalyze the conversion of intracellular hydrogen peroxide into highly toxic hydroxyl radical through a Fenton reaction, which further cleaves thioketal linker of the supramolecular monomer to release potent CPT, thus synergistically amplifying the therapeutic efficacy by combining chemodynamic therapy and chemotherapy. The combination therapy stimulates antitumor immunity and promotes intratumoral infiltration of cytotoxic T lymphocytes by triggering immunogenic cell death. In synergy with PD-L1 checkpoint blockade, **SNPs** enables enhanced immune therapy and a long-term tumor remission.

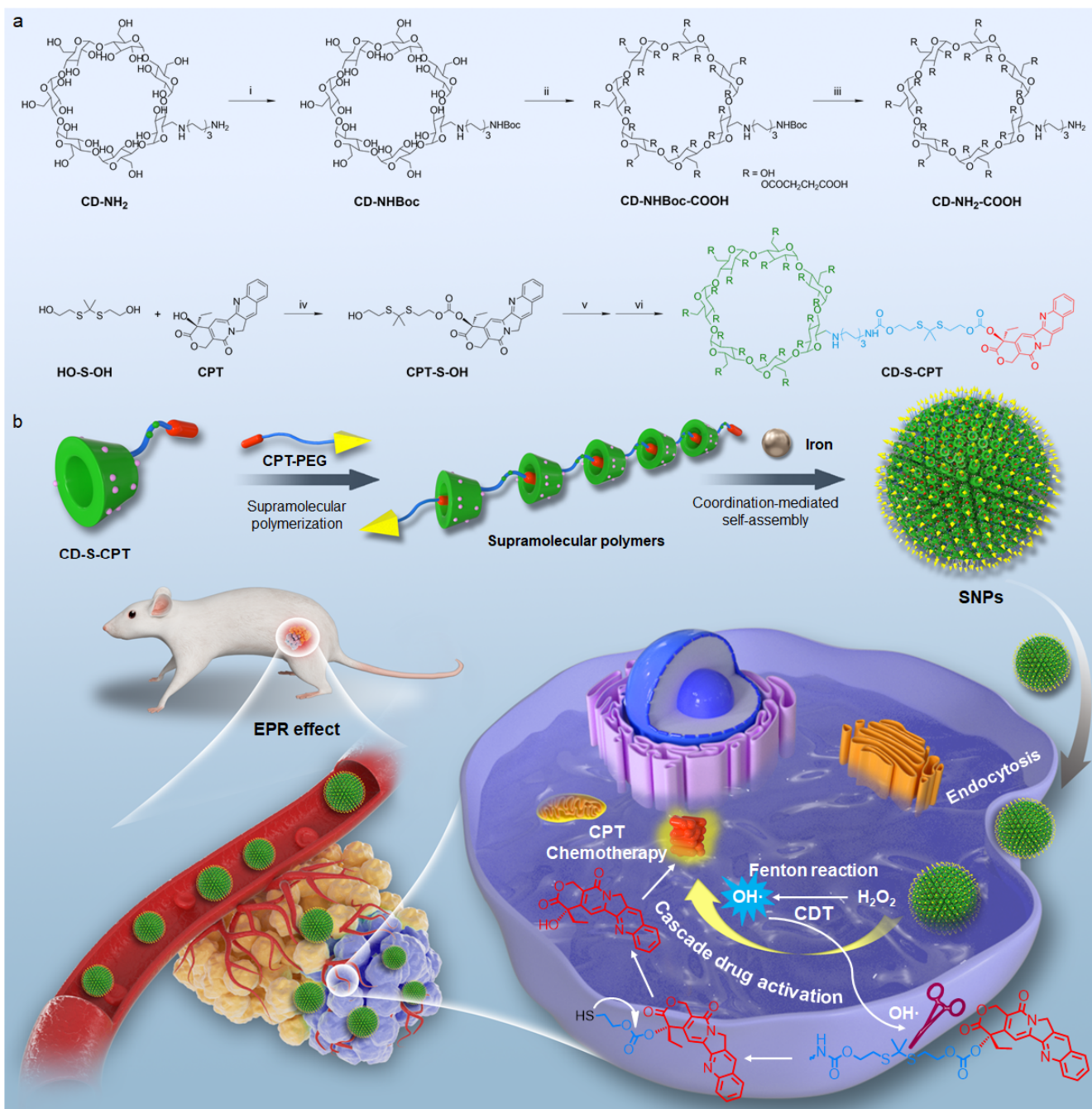
Introduction

Supramolecular nanomedicines prepared from non-covalent interactions have exhibited unparalleled advantages in cancer theranostics, mainly attributing to their dynamic properties and stimuli-responsive capabilities.^[1-8] The pharmacokinetic behaviors, therapeutic performances and undesired side effects of supramolecular nanomedicines can be greatly optimized through supramolecular strategies, which successfully promote their clinical translations.^[9-14] For example, the severe cardiotoxicity faced by doxorubicin is effectively ameliorated and the unsatisfactory antitumor efficacy is greatly promoted by encapsulating the toxic drug in liposomes that are self-assembled from lipids and cholesterol through hydrophobic interactions.^[15] Abraxane, paclitaxel protein-bound particles, significantly

prolongs the circulation half-life and avoids the side effects of paclitaxel by using endogenous albumin as a drug carrier based on the non-covalent interactions in the hydrophobic domain of human serum albumin.^[15] Long-term immunotoxicity mainly arising from the exogenous carriers with poor biodegradability becomes one of the main causes for the failure of traditional nanomedicines in clinical trials, which can also possibly be overcome by rapid excretion of the nanomaterials after drug release through a supramolecular strategy.^[16-19] Although the past decades have demonstrated the bright future of supramolecular nanomedicines, their monotonous therapeutic modality urgently needs to be updated for synergistic therapy aiming to achieving a long-term tumor remission.

Chemodynamic therapy (CDT) utilizing metal ions (e.g., iron, manganese, cobalt and copper) to catalyze endogenous hydrogen peroxide (H_2O_2) into highly toxic hydroxyl radical ($OH\cdot$) through Fenton or Fenton-like reactions to destroy cancer cells remarkably synergizes chemotherapeutic efficacy.^[20-24] The generated $OH\cdot$ not only affects the oxidation of intracellular biomacromolecules including lipids, nucleic acids, and proteins for direct CDT, but also holds the capability to cleave reactive oxygen species (ROS)-responsive bonds to realize on-demand drug release in cancer cells, minimizing unwanted side effects.^[25-27] Indeed, the treatment performances are significantly augmented by combining CDT and chemotherapy attributing to their different anticancer mechanisms, which possibly overcome the inherent limitations faced by traditional chemotherapy.^[28,29] More interestingly, oxidative cell death caused by CDT has been evidenced to involve in eliciting antitumor immune responses by profoundly initiating immunogenic cell death (ICD), which is favorable to reinforce the final therapeutic efficacy.^[30-33]

RESEARCH ARTICLE



Scheme 1. a) Synthetic routes to **CD-S-CPT**. i. di-tert-butyl decarbonate, triethylamine, methanol; ii. succinic anhydride, *N,N*-dimethylformamide; iii. trifluoroacetic acid, methanol; iv. triphosgene, 4-dimethylaminopyridine, dichloromethane; v. 4-nitrophenyl chloroformate, triethylamine, dichloromethane; vi. **CD-NH₂-COOH**, triethylamine, *N,N*-dimethylformamide. b) Scheme illustration of the processes involved in supramolecular nanoparticles (**SNPs**) preparation, *in vivo* delivery, and the cascade-amplified combination CDT and chemotherapy.

Herein, we develop a hybrid supramolecular polymeric nanomedicine with cascade-amplified synergistic efficacy based on β -cyclodextrin/camptothecin (CPT) host-guest molecular recognition and coordination-mediated assembly (Scheme 1). The supramolecular polymer self-assembled from an AB-type monomer is stabilized by iron-carboxylate coordination to afford theranostic supramolecular nanoparticles (**SNPs**). Benefiting from the sophisticated supramolecular engineering and nanotechnology, **SNPs** highly accumulate in tumor sites through the enhanced permeability and retention (EPR) effect. The thioketal linker of **CD-S-CPT** is cleaved inside cancer cells by OH·

produced from a Fenton reaction to release the potent CPT, activating the chemotherapeutic efficacy of **SNPs** (Scheme 1b). Moreover, the combination of CDT and chemotherapy induce an ICD through the release of damage-associated molecular patterns (DAMPs) to elicit immune responses for synergistic therapy. This supramolecular nanomedicine exhibits superior therapeutic efficacy on xenograft and orthotopic tumor models, and its antitumor performance is further promoted combining with anti-PD-L1 (α PD-L1) checkpoint blockade therapy, providing a promising supramolecular nanoplatform for cancer treatments.

RESEARCH ARTICLE

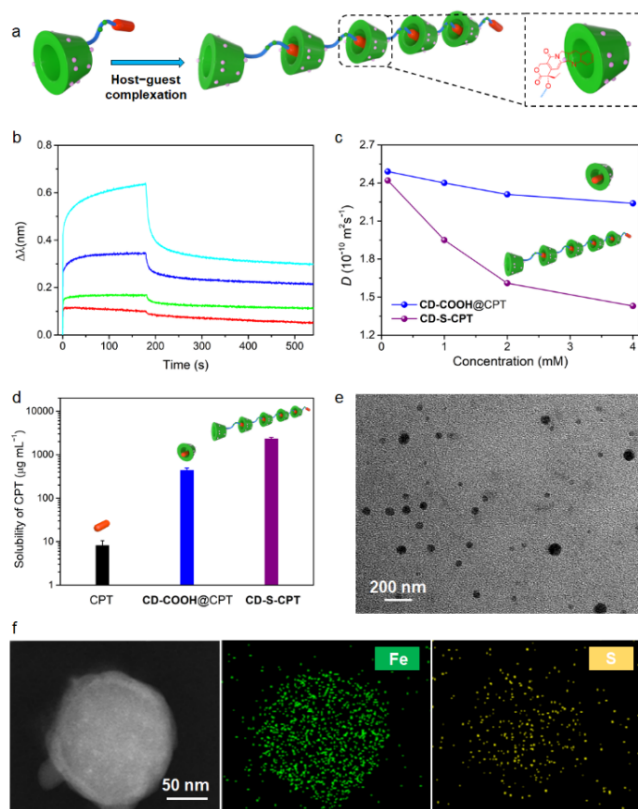


Figure 1. a) Scheme illustration of supramolecular polymerization driven by host-guest complexation. b) The association and dissociation of **CPT-biotin** and **CD-COOH** determined by bi-layer interferometry in PBS. c) Concentration-dependent changes in diffusion coefficient of **CD-S-CPT**. d) Solubility evaluation of **CPT**, **CD-COOH@CPT**, and **CD-S-CPT**. e) TEM image and f) elemental mapping of **SNPs**.

Results and Discussion

The supramolecular monomer **CD-S-CPT** was obtained after six-step syntheses with a high yield and purity (Scheme 1a and Figure S1–13). In order to avoid the reaction between amine and succinic anhydride, **CD-NH₂** was firstly protected by *tert*-butyloxycarbonyl (Boc) group. After the deprotection of Boc-protected amine through a simple carbamate hydrolysis in the presence of trifluoroacetic acid, **CD-NH₂-COOH** was obtained containing multiple carboxylate groups, which provided coordination sites for metals. A ROS-cleavable linker **OH-S-OH** was conjugated to CPT, and the obtained prodrug **CPT-S-OH** was further activated by 4-nitrophenyl chloroformate and reacted with the amine group on **CD-NH₂-COOH** to afford the final supramolecular monomer. The inclusion complexation between β -CD and CPT was verified by 2D NOESY spectroscopy (Figure S24), which indicated that CPT located in the cavity of β -CD (Figure 1a). The binding affinity of this inclusion complex was calculated to be around $1.50 \times 10^4 \text{ M}^{-1}$ by bi-layer interferometry (Figure 1b), which was suitable to prepare supramolecular polymer in aqueous solution. The formation of supramolecular polymeric aggregates was directly validated by determining the concentration-dependent diffusion coefficient, which decreased gradually accompanied with the increase of **CPT-S-OH**

concentration attributing to the supramolecular polymerization (Figure 1c). Due to the severe π - π stacking in aqueous solution (Figure S25), the solubility of CPT is very poor. Interestingly, this supramolecular engineering significantly inhibited the π - π stacking, a 286-fold enhancement in solubility of CPT was achieved by conjugating CPT to the macrocyclic host and forming an inclusion complex (Figure 1a and d). More importantly, the active lactone structure of CPT was significantly kept by forming a host-guest inclusion complex (Figure S26), facilitating to maintain its anticancer ability by this supramolecular strategy.

In order to regulate the self-assembly morphology and improve their stability in physiological environment, **CPT-PEG** was incorporated during supramolecular polymerization. The formed supramolecular diblock polymer exhibited good solubility in aqueous solution, no apparent assemblies were found in transmission electron microscopy (TEM) image (Figure S27). Upon gradual addition of FeCl_3 solution, the supramolecular diblock polymer further aggregated to form nanoparticles driven by the metal-carboxylate coordination (Figure 1e). **SNPs** possessed an average diameter of $122 \pm 10.2 \text{ nm}$ and zeta potential of $9.51 \pm 0.74 \text{ mV}$ (Figure S28–31), which located in the optimized region for tumor accumulation through the EPR effect. The loading contents of CPT and Fe were calculated to be 14.1% and 9.2%, respectively, assuming that all carboxylate groups were fully coordinated. Additionally, the existence of Fe in **SNPs** was verified by TEM-based elemental mapping, in which the Fe and S elements uniformly distributed (Figure 1f). It should be emphasized that the coordination between **CPT-S-CPT** and iron ions in the absence of **CPT-PEG** resulted in the formation of large aggregates due to the intermolecular crosslink (Figure S32).

The chemodynamic effect mediated by iron-triggered Fenton reaction was assessed using methylene blue (MB) as a probe whose absorbance attenuated accompanied with its decomposition by the generated $\text{OH}\cdot$. Figure 2c indicated that the characteristic absorbance of MB solution at 500–700 nm greatly maintained by incubating with **SNPs** alone. The addition of H_2O_2 resulted in a significant diminishment of MB absorbance, and the degradation of MB could be accelerated in the presence of H_2O_2 with a high concentration (Figure S33). The thioketal linker in **CD-S-CPT** was ROS-sensitive, which could be oxidized by highly reactive $\text{OH}\cdot$, thus releasing the active CPT through a cascade reaction (Scheme 1b). As shown in Figure 2d, **SNPs** kept stable in PBS without H_2O_2 , less than 8% of the loaded CPT leaked out from the nanoformulation. In sharp comparison, 68.4% and 85.3% of CPT released from **SNPs** after 48 h incubation in the solution containing 1.00 mM and 5.00 mM of H_2O_2 , respectively, validating the hydroxyl radical-induced drug activation. A non-cleavable supramolecular monomer **CPT-C-CPT** using an alkyl chain as a linker was also synthesized as a control (Figure S14–16). Negligible release of CPT from the supramolecular nanoparticles (**SCNPs**) prepared from **CPT-C-CPT** was observed even in solution containing high-concentrated H_2O_2 , further demonstrating that the thioketal bond played a pivotal role in drug activation (Figure 2d).

RESEARCH ARTICLE

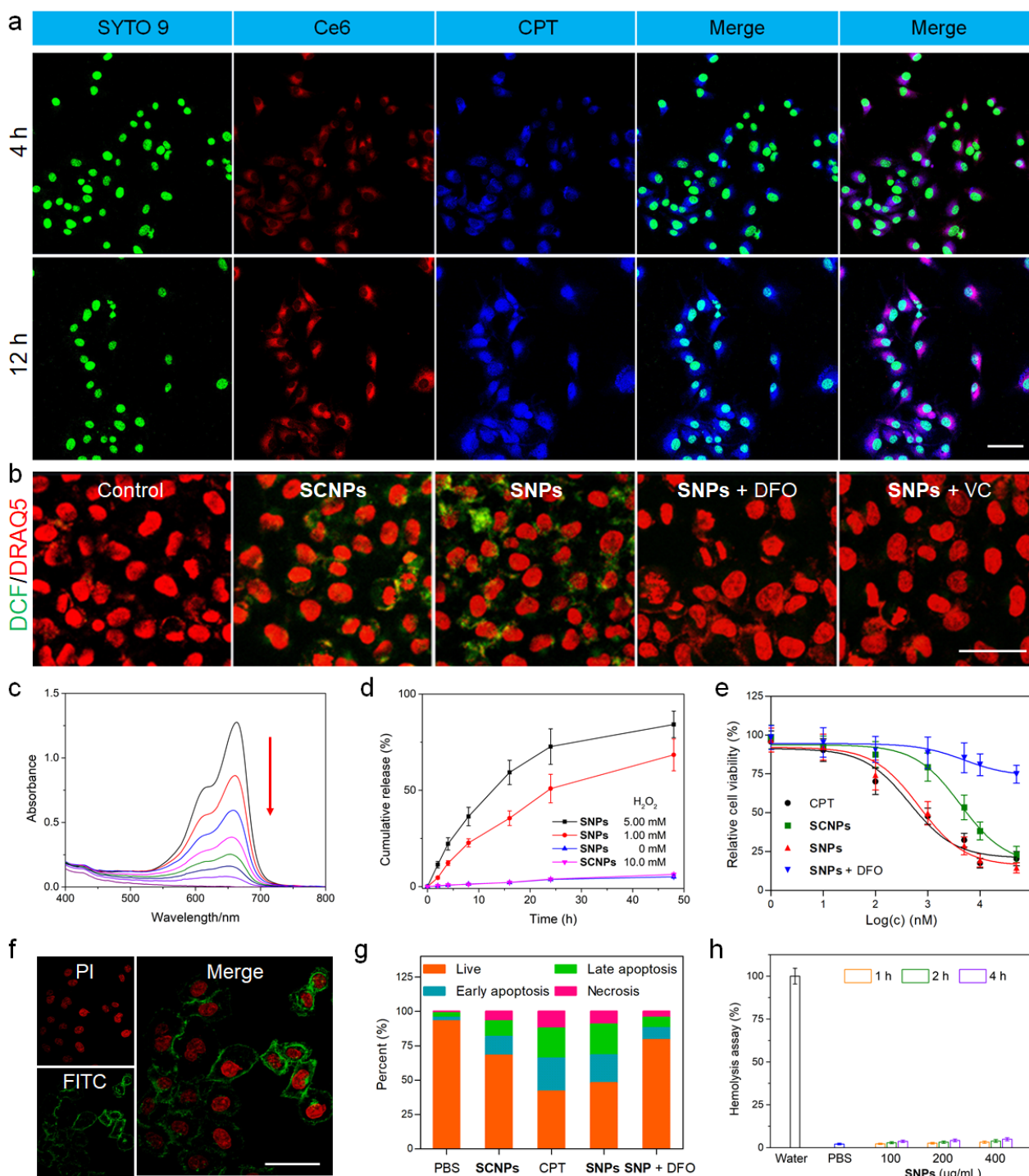


Figure 2. a) CLSM images of 4T1 cells incubated with **SNPs@Ce6** for 4 h and 12 h, respectively. Scale bar: 50 μm . b) CLSM images of intracellular ROS (DCF, green) generation in 4T1 cells under different treatments. Scale bar: 50 μm . c) The absorption changes of the MB solution containing **SNPs** in the presence of H_2O_2 (5.00 mM). d) Cumulative release curves of CPT from **SCNPs** or **SNPs** in solutions containing different concentrations of H_2O_2 . e) Cytotoxicity evaluation of 4T1 cells after 48 h incubation with CPT, **SCNPs**, **SNPs**, or **SNPs + DFO**. f) CLSM images of annexin V-FITC/PI contained 4T1 cells after 48 h of exposure to **SNPs**. Scale bar: 50 μm . g) Annexin-V/PI assay of 4T1 cells after different treatments. h) Hemolysis assay of **SNPs** at various concentrations.

In order to trace the intracellular translocation of **SNPs** after internalization by 4T1 cancer cells, a fluorophore chlorin e6 (Ce6) containing three carboxylate groups was successfully incorporated into the **SNPs** by taking advantage of coordination interactions. Confocal laser scanning microscopy (CLSM)

revealed that **SNPs** were effectively internalized by 4T1 cells, red fluorescence arising from Ce6-loaded **SNPs** (**SNPs@Ce6**) was observed in cytoplasm after 4 h incubation (Figure 2a and Figure S34). Intracellular generation of ROS was monitored using an activatable probe, 2,7-dichlorofluorescein diacetate, whose

RESEARCH ARTICLE

fluorescence lights up after being oxidized into highly emissive 2,7-dichlorofluorescein (Figure 2b). Quantitative measurements indicated that 35.2-fold enhancement in green fluorescence was achieved for the cells treated with **SNPs** (Figure S35 and Figure S36), whereas the amplification effect remarkably attenuated by pre-treating 4T1 cells with an iron chelator (deferoxamine mesylate, DFO) and a ROS scavenger (vitamin C, VC), demonstrating that iron ions in **SNPs** were able to trigger a Fenton reaction inside cells. Blue fluorescence from CPT was found in nucleus after 4 h incubation and the signal intensified by extending the incubation time to 12 h (Figure 2a), because the generated OH \cdot oxidized the thioketal group to release active CPT, which translocated to the site of action. The anticancer efficacy was evaluated using an MTT assay. **SNPs** exhibited outstanding anticancer capability, the half maximal inhibitory concentration (IC₅₀) of **SNPs** was determined to be $0.68 \pm 0.07 \mu\text{M}$ (Figure 2e). Pre-treatment with DFO greatly impaired the anticancer efficacy, the IC₅₀ value increased to $4.91 \pm 0.36 \mu\text{M}$. Annexin V-FITC/PI dual-staining showed that green fluorescence on membrane and red fluorescence in nucleus were observed for the apoptotic cells after incubation with **SNPs** (Figure 2f). It was demonstrated that **SNPs**-mediated combination therapy greatly induced the apoptosis and necrosis, the apoptotic and necrotic ratios were quantitatively determined to be 40.7% and 9.6% (Figure 2g). The apoptosis was inhibited by co-culturing 4T1 cells with **SNPs** in the presence of DFO due to the attenuation of CDT and ROS-triggered drug activation. These studies verified that **SNPs** stabilized by host-guest recognition and coordination-mediated assembly could be used for cascade-amplified synergetic cancer therapy.

Hemolysis assay confirmed the good biosafety of **SNPs** for *in vivo* utilizations, the hemolysis percentage of red blood cells located within the negligible scope as **SNPs** concentration increased in the range 100–400 $\mu\text{g/mL}$ (Figure 2h). The blood circulation half-life of **SNPs@Ce6** was determined to be $1.65 \pm 0.17 \text{ h}$ by detecting the fluorescence signal in blood after different time post intravenous (*i.v.*) injection (Figure S37). As a control, free CPT was rapidly eliminated from blood, which suggested the supramolecular nanoformulation successfully prolonged the circulation time. Fluorescence imaging was employed to trace the delivery of this hybrid supramolecular nanomedicine *in vivo* using **SNPs@Ce6**. As shown in Figure 3a, fluorescence signal was observed in tumor at 2 h post injection, the intensity was progressively strengthened at 8, 16 and 24 h post injection, a convincing evidence for the high tumor accumulation of **SNPs@Ce6**. Quantitative analysis indicated the intratumoral fluorescence increased gradually post *i.v.* injection of **SNPs@Ce6** (Figure 3b), further evidencing that this nanomedicine highly accumulated in the tumor. Notably, exceptionally intensive signal was visible in the tumor area for more than 48 h in comparison with other tissues. *Ex vivo* imaging also validated high tumor

accumulation of **SNPs@Ce6**, the excised tumor exhibited stronger fluorescence intensity than other organs (Figure 3c). More importantly, strong red signal was detected in the tumor tissue and distributed homogeneously whole of the tumor, an evidence of high tumor penetration of **SNPs@Ce6** (Figure 3d).

The cascade-amplified synergetic cancer therapy combining CDT and chemotherapy was assessed on nude mice bearing 4T1 tumor. For the control group administrated with PBS, no therapeutic benefit was observed and the tumor volume increased rapidly (Figure 3e). The mice treated with **SCNPs** resulted in unsatisfactory antitumor efficacy, because their chemotherapeutic effect was hampered using a non-cleavable linker. Although free CPT exhibited moderate antitumor outcomes and the tumor growth was suppressed in the first days during therapy, the systemic toxicity was severe. Ascribing to the excellent anticancer efficacy, the administration of **SNPs** greatly extended the survival time (Figure 3f). The body weight of the mice received CPT formulation dropped remarkably (Figure S38), and obvious symptoms of systemic toxicity were found during therapeutic period, including eating, activity, and grooming. Noteworthy, the administration of **SNPs** remarkably suppressed the tumor growth, confirming the superior antitumor performance combining CDT and chemotherapy. Correspondingly, the tumor inhibition was 18.7%, 42.5%, and 74.8% for **SCNPs**, CPT, and **SNPs**, respectively (Figure S39). The superior antitumor outcome of **SNPs** was further validated by hematoxylin and eosin (H&E) staining (Figure 3h) and transferase-mediated dUTP nick end-labeling (TUNEL) staining (Figure 3i). The highest level of apoptotic/necrotic cells was observed in the tumor section from the mice treated with **SNPs** among these groups, and the apoptosis ratio was calculated as high as 76.3% according to TUNEL staining attributing to the synergistic efficacy, which was much higher than the other treatments (Figure 3g).

Oxidative cell death caused by CDT has been evidenced to induce ICD, thus stimulating an immune response to inhibit tumor growth and increase tumor infiltrating lymphocytes (TILs).^[34–36] Inspired by the outstanding antitumor performance of **SNPs** combining CDT and chemotherapy on a nude mice model, **SNPs** was further employed to synergize with immune checkpoint blockade aiming to boosting the antitumor immunity for a long-term tumor suppression (Figure 4a). DAMPs, including calreticulin (CRT), high mobility group protein B1 (HMGB1), and ATP, released from dying cancer cells were quantitatively measured for the cells after different treatments. Strong red fluorescence derived from CRT was detected in CLSM images for 4T1 cells cultured with **SNPs** (Figure 4b and Figure S40). The ratio of CRT-positive cells was quantitatively measured to be $6.41 \pm 0.8\%$, $23.7 \pm 1.8\%$, $29.3 \pm 3.1\%$, $50.8 \pm 6.1\%$, and $18.4 \pm 2.2\%$ after the treatment with PBS, CPT, **SCNPs**, **SNPs**, and **SNPs** + DFO, respectively (Figure 4c).

RESEARCH ARTICLE

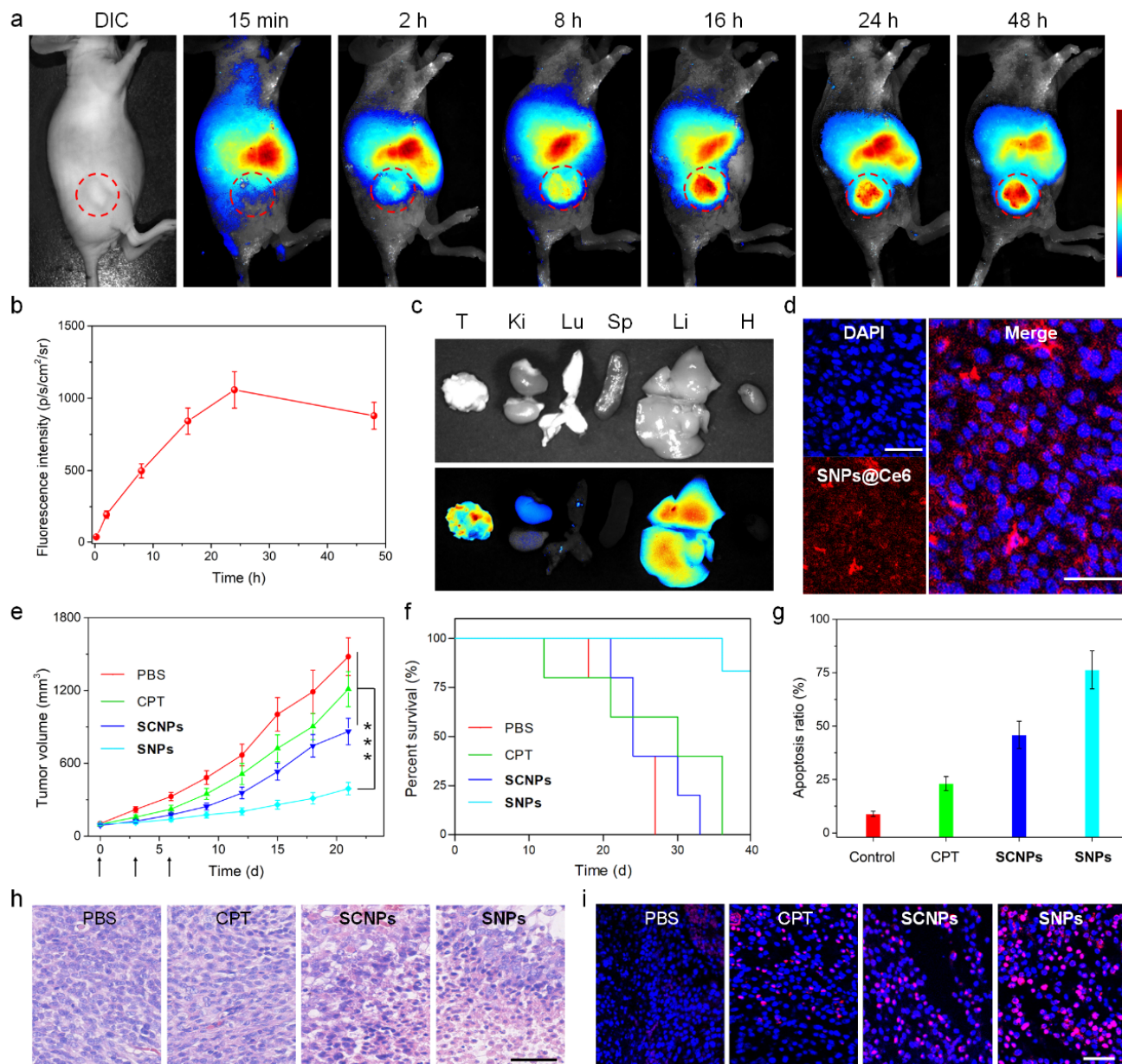


Figure 3. a) Fluorescence imaging of the mice bearing 4T1 tumor after *i.v.* injection of **SNPs@Ce6**. b) Time-dependent changes of intratumoral fluorescence intensity after injection of **SNPs@Ce6**. c) *Ex vivo* fluorescence imaging of main organs harvested from the mice at 48 h post injection of **SNPs@Ce6**. d) CLSM image of the tumor slice from the mice treated with **SNPs@Ce6** at 24 h post injection. Scale bar: 100 μm . e) Tumor growth curves and f) survival ratio of the mice administrated with different formulations. *** $p < 0.001$. g) Apoptosis ratio in tumor sites from the mice after different treatments. h) H&E and i) TUNEL staining of the tumor tissues from the mice after different treatments. Scale bar: 200 μm .

HMGB1 was primarily distributed in nucleus, while the majority of HMGB1 released with the aid of **SNPs**-mediated CDT and chemotherapy, as verified by the attenuation of fluorescent signal in nucleic area (Figure 4d and Figure S41). HMGB1 secretion from the nucleus to the extracellular environment was essential to stimulate antigen presentation to T cells, enhancing the antitumor immunity. Moreover, 4T1 cells incubated with **SNPs** induced the pro-apoptotic ATP release, the ATP amount in extracellular culture was 2.23-, 1.76-, and 2.39-fold higher than the cells treated with CPT, **SCNPs**, and **SNPs** + DFO (Figure 4e). ATP acting as a "find me" signal elicited immune response by activating dendritic cells (DCs). The percentage of matured DCs

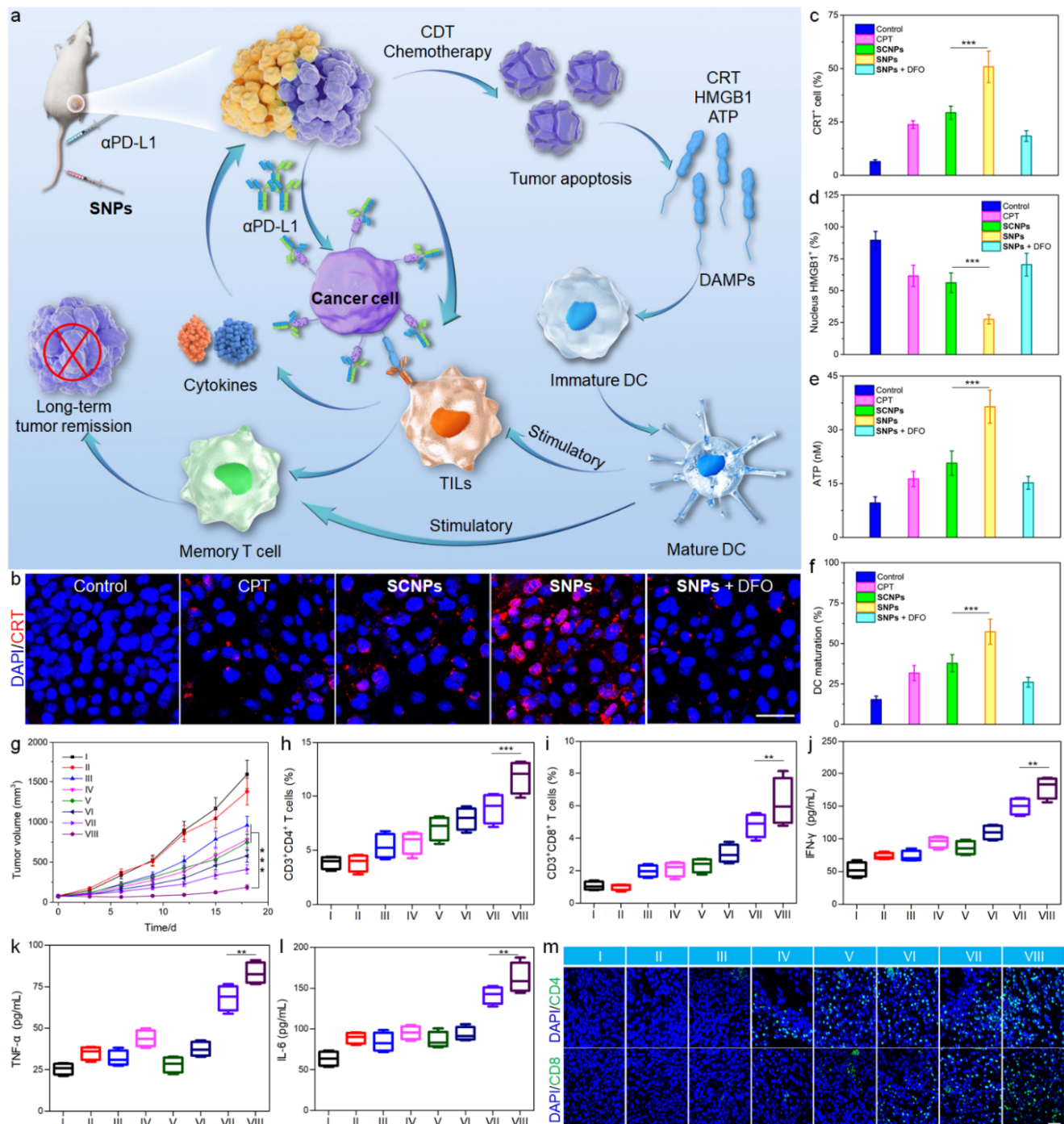
significantly increased to 57.3% after co-culture with the 4T1 cells treated with **SNPs** (Figure 4f). These results demonstrated that this supramolecular nanomedicine possessed the capability to induce ICD and further stimulate antitumor immunity, conferring **SNPs** an excellent therapeutic effect by boosting antitumor immunity.

An orthotopic breast tumor model was established on Balb/c mice to assess the antitumor efficacy of **SNPs** synergized with immune checkpoint blockade. Figure 4g indicated that free $\alpha\text{PD-L1}$ and **SCNPs** were invalid against this triple-negative breast cancer, the tumors grew rapidly for the mice administrated with $\alpha\text{PD-L1}$ and **SCNPs**. The tumor growth minorly delayed for the

RESEARCH ARTICLE

mice formulated with **SNPs** + α PD-L1, attributing to the limited chemotherapeutic efficacy of this non-responsive nanomedicine. The combination of CDT and chemotherapy exhibited more effective antitumor outcome, the administration of **SNPs** effectively inhibited tumor growth in early days during therapy. However, the tumor relapsed at later time points. Excitingly, the formulation of **SNPs** + α PD-L1 exhibited the most significant

inhibition of tumor growth and no tumor relapse occurred throughout the therapeutic period. Tumor weight measurement and H&E staining also revealed that the administration of **SNPs** + α PD-L1 resulted in the highest level of apoptotic and necrotic cancer cells in tumor tissues in comparison with other formulations (Figure S42 and Figure S43).



RESEARCH ARTICLE

To investigate the contribution of immune response to the therapeutic outcome, tumor tissues were harvested and the immunostimulatory activity was evaluated by immunofluorescence assay. Compared with other groups, **SNPs** treatments (**SNPs** and **SNPs** + α PD-L1) induced high level of CRT exposure and evoked large amount of HMGB1 in the extracellular environment (Figure S44 and Figure S45), indicating these DAMPs possibly promoted immune recognitions and activated antitumor immunotherapy. Compared with the PBS-treated group, the treatments of free α PD-L1, CPT, CPT + α PD-L1, **SCNPs**, and **SCNPs** + α PD-L1 moderately facilitated the DC maturation to $13.6 \pm 1.1\%$, $23.3 \pm 1.9\%$, $24.8 \pm 2.3\%$, $21.1 \pm 1.7\%$, and $24.3 \pm 3.1\%$, respectively (Figure S46). On the contrary, matured frequency of DCs increased to $39.6 \pm 3.4\%$ for the mice treated with **SNPs**. **SNPs** + α PD-L1 dramatically stimulated DC maturation up to $46.7 \pm 5.1\%$, which was 3.43- and 1.92-fold as those of free α PD-L1 and **SCNPs** + α PD-L1, respectively.

The intratumor infiltration of T lymphocytes was evaluated by CLSM and flow cytometric detection. Figure 4m confirmed the amounts of intratumoral CD4⁺ T and CD8⁺ T cells were upregulated for the mice treated with **SNPs** + α PD-L1, while the immunosuppressive regulatory T cells (Tregs) was down-regulated (Figure S47). Quantitatively, the frequency of infiltrating CD4⁺ and CD8⁺ T cells was measured to be 11.8% and 6.24% in the group administrated with **SNPs** + α PD-L1 (Figure 4h and I), much higher than those in the other groups. The administration of **SNPs** + α PD-L1 increased the CD8⁺ T cells to Tregs ratio by 2.88- and 47.2-fold in comparison with **SNPs** and α PD-L1, respectively (Figure S48), implying **SNPs** greatly elicited antitumor immune response combining with immune checkpoint blockade. Enzyme-linked immunosorbent assays was employed to measure the intratumoral cytokines attributing to DCs maturation-induced systemic immune responses. T cell-derived cytokines, including interferon- γ (IFN- γ), tumor necrosis factor- α (TNF- α), interleukin-6 (IL-6), and IL-12, upregulated after the treatment of **SNPs** + α PD-L1 (Figure 4j-l and Figure S49), indicating a robust immune response through **SNPs**-triggered ICD and adjunctive immune checkpoint blockade. The decreased secretion of immune-suppressive cytokine, transforming growth factor- β (TGF- β), was also found in the **SNPs** + α PD-L1 group, representing the attenuation of immunosuppression after combination therapy (Figure S50).

The systemic toxicity of **SNPs** was assessed by recording the changes in body weight within therapeutic period. Due to the non-specific biodistribution and poor solubility of CPT, the administration of free CPT and CPT + α PD-L1 resulted in severe side effect (Figure S51), as indicated by the significant weight loss and mice death during therapy. In contrast, no obvious body weight variation was detected for the mice administrated with **SNPs**. H&E staining of major organs indicated that no obvious tissue damage, accumulation of inflammatory immune cells and inflammatory lesion were detected in the mice treated with **SNPs** + α PD-L1 as compared with healthy mice (Figure S52). Moreover, no detectable abnormality was observed in the key indexes of hepatotoxicity and nephrotoxicity, such as alanine

aminotransferase, aspartate aminotransferase, alkaline phosphatase, blood urine nitrogen, creatinine, uric acid (Figure S44). Routine blood analysis also verified that other hematological parameters were all in normal range (Figure S53), demonstrating low systemic toxicity of this hybrid supramolecular nanomedicine, which was crucial for *in vivo* biomedical applications.

Conclusion

In summary, we developed a hybrid supramolecular nanomedicine prepared from host-guest molecular recognition and coordination-mediated assembly for cascade-amplified synergetic cancer therapy. Iron ions stabilizing **SNPs** acted as catalyst to generate highly active OH \cdot by catalyzing the intracellular H₂O₂ through a Fenton reaction, which not only acted as a toxic agent for CDT but also was used to cleave the thioketal linker of supramolecular monomer to release active CPT, thus realizing combination therapy combining CDT and chemotherapy. Benefiting from sophisticated nanotechnology and supramolecular engineering, the solubility and pharmacokinetic behaviors were effectively promoted, resulting in high tumor accumulation of **SNPs** through the EPR effect. The formulation of **SNPs** exhibited excellent antitumor performance, the tumor growth was suppressed after receiving this supramolecular nanomedicine on xenograft and orthogonal tumor models. Intriguingly, the combination of CDT and chemotherapy achieved an intense ICD effect to remodel the tumor immunomicroenvironment, promoting the proliferation and activity of tumor-specific effector T cells. More importantly, in synergy with immune checkpoint blockade, the activation of systemic immune response significantly augmented the long-term inhibition of tumors without relapse. This state-of-the-art paradigm implies a meaningful insight of utilizing supramolecular nanomedicine for synergistic treatments and inspires sophisticated nanomedicines for clinical trials.

Acknowledgements

This work was supported by the Tsinghua University Spring Breeze Fund (2021Z99CFZ007), the startup funding by Tsinghua University, the National Natural Science Foundation of China (22175107), and the Starry Night Science Fund of Zhejiang University Shanghai Institute for Advanced Study (SN-ZJU-SIAS-006).

Competing financial interests

The authors declare no competing financial interests.

Keywords: cancer theranostics • chemodynamic therapy • host-guest systems • immunotherapy • supramolecular chemistry

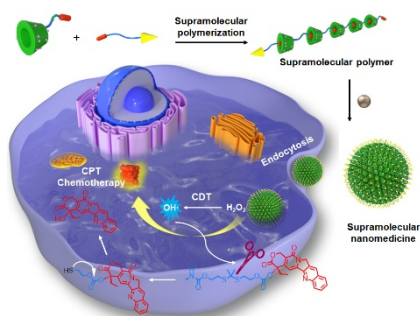
[1] M. E. Davis, M. E. Brewster, *Nat. Rev. Drug Discov.* **2004**, *3*, 1023–1035.

RESEARCH ARTICLE

- [2] J. Zhou, L. Rao, G. Yu, T. R. Cook, X. Chen, F. Huang, *Chem. Soc. Rev.* **2021**, *50*, 2839–2891.
- [3] J. Park, S. H. Wrzesinski, E. Stern, M. Look, J. Criscione, R. Ragheb, S. M. Jay, S. L. Demento, A. Agawu, P. L. Limon, A. F. Ferrandino, D. Gonzalez, A. Habermann, R. A. Flavell, T. M. Fahmy, *Nat. Mater.* **2012**, *11*, 895–905.
- [4] H. Cabral, N. Nishiyama, K. Kataoka, *Acc. Chem. Res.* **2011**, *44*, 999–1008.
- [5] X. Ma, Y. Zhao, *Chem. Rev.* **2015**, *115*, 7794–7839.
- [6] M. J. Webber, R. Langer, *Chem. Soc. Rev.* **2017**, *46*, 6600–6620.
- [7] L. Wang, L. Li, Y. Fan, H. Wang, *Adv. Mater.* **2013**, *25*, 3888–3898.
- [8] A. J. Clark, D. T. Wiley, J. E. Zuckerman, P. Webster, J. Chao, J. Lin, Y. Yen, M. E. Davis, *Proc. Natl. Acad. Sci. USA* **2016**, *113*, 3850–3854.
- [9] C. B. Rodell, S. P. Arlauckas, M. F. Cuccarese, C. S. Garris, R. Li, M. S. Ahmed, R. H. Kohler, M. J. Pittet, R. Weissleder, *Nat. Biomed. Eng.* **2018**, *2*, 578–588.
- [10] J. Zhou, G. Yu, F. Huang, *Chem. Soc. Rev.* **2017**, *46*, 7021–7053.
- [11] Y.-M. Zhang, Y.-H. Liu, Yu Liu, *Adv. Mater.* **2019**, *32*, 1806158.
- [12] H. Chen, X. Zeng, H. P. Tham, S. Z. F. Phua, W. Cheng, W. Zeng, H. Shi, L. Mei, Y. Zhao, *Angew. Chem. Int. Ed.* **2019**, *58*, 7641–7646; *Angew. Chem.* **2019**, *131*, 7723–7728.
- [13] Z. Li, N. Song, Y.-W. Yang, *Matter* **2019**, *1*, 345–368.
- [14] J. Zhang, P. X. Ma, *Adv. Drug Delivery Rev.* **2013**, *65*, 1215–1233.
- [15] Y. Min, J. M. Caster, M. J. Eblan, A. Z. Wang, *Chem. Rev.* **2015**, *115*, 11147–11190.
- [16] M. Elsbahy, K. L. Wooley, *Acc. Chem. Res.* **2015**, *48*, 1620–1630.
- [17] M. A. Dobrovolskaia, D. R. Germolec, J. L. Weaver, *Nat. Nanotechnol.* **2009**, *4*, 411–414.
- [18] K. Yang, G. Yu, Z. Yang, L. Yue, X. Zhang, C. Sun, J. Wei, L. Rao, X. Chen, R. Wang, *Angew. Chem. Int. Ed.* **2021**, *60*, 17570–17578; *Angew. Chem.* **2021**, *133*, 17711–17719.
- [19] G. Yu, X. Zhao, J. Zhou, Z. Mao, X. Huang, Z. Wang, B. Hua, Y. Liu, F. Zhang, Z. He, O. Jacobson, C. Gao, W. Wang, C. Yu, X. Zhu, F. Huang, X. Chen, *J. Am. Chem. Soc.* **2018**, *140*, 8005–8019.
- [20] Z. Tang, P. Zhao, H. Wang, Y. Liu, W. Bu, *Chem. Rev.* **2021**, *121*, 1981–2019.
- [21] B. Ding, P. Zheng, F. Jiang, Y. Zhao, M. Wang, M. Chang, P. Ma, J. Lin, *Angew. Chem. Int. Ed.* **2020**, *59*, 16381–16384; *Angew. Chem.* **2020**, *132*, 16523–16526.
- [22] W. Bao, M. Liu, J. Meng, S. Liu, S. Wang, R. Jia, Y. Wang, G. Ma, W. Wei, Z. Tian, *Nat. Commun.* **2021**, *12*, 6399.
- [23] Z. Ren, S. Sun, R. Sun, G. Cui, L. Hong, B. Rao, A. Li, Z. Yu, Q. Kan, Z. Mao, *Adv. Mater.* **2020**, *32*, 1906024.
- [24] H. Lin, Y. Chen, J. Shi, *Chem. Soc. Rev.* **2018**, *47*, 1938–1958.
- [25] S. Wang, G. Yu, Z. Wang, O. Jacobson, L.-S. Lin, W. Yang, H. Deng, Z. He, Y. Liu, Z.-Y. Chen, X. Chen, *Angew. Chem. Int. Ed.* **2019**, *58*, 14758–14763; *Angew. Chem.* **2019**, *131*, 14900–14905.
- [26] P. Sun, Q. Deng, L. Kang, Y. Sun, J. Ren, X. Qu, *ACS Nano* **2020**, *14*, 13894–13904.
- [27] J. Tan, X. Duan, F. Zhang, X. Ban, J. Mao, M. Cao, S. Han, X. Shuai, J. Shen, *Adv. Sci.* **2020**, *7*, 2003036.
- [28] W. Ke, J. Li, F. Mohammed, Y. Wang, K. Tou, X. Liu, P. Wen, H. Kinoh, Y. Anraku, H. Chen, K. Kataoka, Z. Ge, *ACS Nano* **2019**, *13*, 2357–2369.
- [29] B. Yang, Y. Chen, J. Shi, *Chem. Rev.* **2019**, *119*, 4881–4985.
- [30] D. R. Green, T. Ferguson, L. Zitvogel, G. Kroemer, *Nat. Rev. Immunol.* **2009**, *9*, 353–363.
- [31] H. Deng, W. Yang, Z. Zhou, R. Tian, L. Lin, Y. Ma, J. Song, X. Chen, *Nat. Commun.* **2020**, *11*, 4951.
- [32] Y. Liu, W. Zhen, Y. Wang, S. Song, H. Zhang, *J. Am. Chem. Soc.* **2020**, *142*, 21751–21757.
- [33] Z. Liu, W. Jiang, J. Nam, J. J. Moon, B. Y. S. Kim, *Nano Lett.* **2018**, *18*, 6655–6659.
- [34] D. V. Krysko, A. D. Garg, A. Kaczmarek, O. Krysko, P. Agostinis, P. Vandenabeele, *Nat. Rev. Cancer* **2012**, *12*, 860–875.
- [35] P. Zhang, Y. Zhai, Y. Cai, Y. Zhao, Y. Li, *Adv. Mater.* **2019**, *31*, 1904156.
- [36] A. Gao, B. Chen, J. Gao, F. Zhou, M. Saeed, B. Hou, Y. Li, H. Yu, *Nano Lett.* **2020**, *20*, 353–362.

RESEARCH ARTICLE

Table of Contents



A hybrid supramolecular polymeric nanomedicine for cascade-amplified synergetic chemodynamic therapy and chemotherapy is constructed based on β -cyclodextrin/camptothecin host-guest molecular recognition and iron-carboxylate coordination. In synergy with a checkpoint blockade, this supramolecular nanomedicine leads to an enhanced therapeutic performance and a long-term tumor remission.

Accepted Manuscript